

# Physics potential for the measurement of $\sigma(H\nu\bar{\nu}) \times \text{BR}(H \rightarrow \mu^+\mu^-)$ at the 1.4 TeV CLIC collider

G. Milutinović-Dumbelović<sup>1,a</sup>, I. Božović-Jelisavčić<sup>1</sup>, C. Greife<sup>2,3</sup>, G. Kačarević<sup>1</sup>,  
S. Lukić<sup>1</sup>, M. Pandurović<sup>1</sup>, P. Roloff<sup>3</sup>, I. Smiljanić<sup>1</sup>

<sup>1</sup> Vinca Institute of Nuclear Sciences, University of Belgrade, Mihajla Petrovića Alasa 12-14, 11001 Belgrade, Serbia

<sup>2</sup> Universität Bonn, 53012 Bonn, Germany

<sup>3</sup> CERN, 1211 Geneva 23, Switzerland

Received: 24 July 2015 / Accepted: 19 October 2015 / Published online: 30 October 2015

© The Author(s) 2015. This article is published with open access at Springerlink.com

**Abstract** The future compact linear collider (CLIC) offers a possibility for a rich precision physics programme, in particular in the Higgs sector through the energy staging. This is the first paper addressing the measurement of the standard model Higgs boson decay into two muons at 1.4 TeV CLIC. With respect to similar studies at future linear colliders, this paper includes several novel contributions to the statistical uncertainty of the measurement. The latter includes the equivalent photon approximation employed to describe  $e^+e^-$  and  $e\gamma$  interactions whenever the virtuality of the mediated photon is smaller than 4 GeV and realistic forward electron tagging based on energy deposition maps in the forward calorimeters, as well as several processes with the Beamstrahlung photons that results in irreducible contribution to the signal. In addition, coincidence of the Bhabha scattering with the signal and background processes is considered, altering the signal selection efficiency. The study is performed using a fully simulated CLIC\_ILD detector model. It is shown that the branching ratio for the Higgs decay into a pair of muons  $\text{BR}(H \rightarrow \mu^+\mu^-)$  times the Higgs production cross-section in  $WW$ -fusion  $\sigma(H\nu\bar{\nu})$  can be measured with 38 % statistical accuracy at  $\sqrt{s} = 1.4$  TeV, assuming an integrated luminosity of  $1.5 \text{ ab}^{-1}$  with unpolarised beams. If 80 % electron beam polarisation is considered, the statistical uncertainty of the measurement is reduced to 25 %. Systematic uncertainties are negligible in comparison to the statistical uncertainty.

## 1 Introduction

Measurements of Higgs branching ratios, and consequently Higgs couplings, provide a strong test of the standard model (SM) and possible physics beyond. Models that could possibly extend the SM Higgs sector (Two Higgs Doublet model, Little Higgs models or Compositeness models) will require Higgs couplings to electroweak bosons and Higgs-fermion Yukawa couplings (coupling-mass linearity) to deviate from the SM predictions [1,2].

The compact linear collider (CLIC) represents an excellent environment to study properties of the Higgs boson, including its couplings, with a very high precision [3,4]. Measurements of rare  $H \rightarrow \mu^+\mu^-$  decays are particularly challenging because of the very low branching ratio of  $2 \times 10^{-4}$  predicted in the SM [5] for a Higgs mass of 126 GeV. Current results indicate that the LHC was not able to access Higgs coupling to muons ( $g_{H\mu\mu}$ ), based on the runs at 7 TeV and 8 TeV centre-of-mass (CM) energies [6]. Projections for the HL-LHC, assuming  $300 \text{ fb}^{-1}$  and  $3 \text{ ab}^{-1}$  of data, predict uncertainties of 23 and 8 % respectively for the  $g_{H\mu\mu}$  coupling [7]. In order to provide the best physics reach in the shortest time and for an optimal cost, the operation of the CLIC accelerator is foreseen in energy stages of 350 GeV, 1.4 and 3 TeV [8]. At 1.4 and 3 TeV, sufficiently large Higgs boson samples can be produced to allow studies of rare Higgs decays. A sample of  $3.7 \times 10^5$  Higgs bosons can be produced at 1.4 TeV CM energy, for an integrated luminosity of  $1.5 \text{ ab}^{-1}$  with unpolarised beams. With the expected instantaneous luminosity of  $3.2 \times 10^{34} \text{ cm}^{-2} \text{ s}^{-1}$  this can be achieved in approximately five years of detector operation, with 200 running days per year and an effective up-time of 50 % [9]. The signal sample size will be doubled at 3 TeV CM energy due to rising cross-section for  $WW$ -fusion [10].

This work was carried out in the framework of the CLICdp collaboration.

<sup>a</sup> e-mail: [gordanamd@vinca.rs](mailto:gordanamd@vinca.rs)

A similar study has been performed at 3 TeV CM energy [10]. Compared to the study at 3 TeV, several challenges for the measurement of  $H \rightarrow \mu^+\mu^-$  at CLIC are discussed for the first time in this paper. First, background processes with photons in the initial state simulated using both the expected Beamstrahlung spectrum at CLIC and the equivalent photon approximation (EPA) [11, 12], were considered. Forward electron tagging (Sect. 5) leads to a rejection of 48 and 42 % of the  $e^-e^+ \rightarrow e^-e^+\mu^+\mu^-$  and  $e^\pm\gamma \rightarrow e^\pm\mu^+\mu^-$  background events, respectively. The impact of Bhabha scattering events on the rejection of events with forward electrons is investigated.

The paper is organised as follows. In Sect. 2 the simulation tools used for the analysis are listed and in Sect. 3 the CLIC\_ILD detector model is briefly described. Signal and background processes and event samples are discussed in Sect. 4. Tagging of background high-energy electrons is described in Sect. 5. Event preselection and the final selection based on a multivariate analysis (MVA) approach are described in Sect. 6. The di-muon invariant mass fit and the extraction of the statistical uncertainty of the measurement are described in Sect. 7. In Sect. 8 the impact of electron polarisation on the statistical uncertainty of the  $\sigma(H\nu\bar{\nu}) \times \text{BR}(H \rightarrow \mu^+\mu^-)$  measurement is described. Systematic uncertainties are discussed in Sect. 9, followed by the conclusions in Sect. 10.

## 2 Simulation and analysis tools

Higgs production through  $WW$ -fusion is simulated in Whizard 1.95 [13, 14] including a realistic CLIC beam spectrum and initial state radiation. The generator Pythia 6.4 [15] is used to simulate the Higgs decay into two muons. The CLIC luminosity spectrum and beam-induced processes are obtained by GuineaPig 1.4.4 [16]. Background events are also generated with Whizard using Pythia 6.4 to simulate the hadronization and fragmentation processes. Simulation of tau decays is done by Tauola [17]. The CLIC\_ILD detector simulation is performed using Mokka [18] based on Geant4 [19]. Before digitisation of the detector signals, pile-up from  $\gamma\gamma \rightarrow$  hadrons interactions is overlaid on the physics events. The particle flow algorithm, PandoraPFA [20, 21] is employed in reconstruction of the final-state particles within the Marlin reconstruction framework [22]. The TMVA package [23] is used to separate signal from background by MVA of signal and background kinematic properties.

## 3 The CLIC\_ILD detector model

The ILD detector concept [24] is modified for CLIC according to the specific experimental conditions at higher energies

[3]. The subsystems of particular relevance for the presented analysis are discussed here. A complete description of the CLIC\_ILD detector can be found in [25].

The main tracking device of CLIC\_ILD is the Time Projection Chamber (TPC) providing a point resolution in the  $r\phi$  plane better than 100  $\mu\text{m}$ , for charged particles in the detector angular acceptance [3]. Additional silicon trackers cover polar angles down to  $7^\circ$ . They have a single point resolution of 7  $\mu\text{m}$ , and together with the TPC improve the tracking accuracy in the  $r\phi$  plane. In order to provide precision tracking and vertexing closer to the beam-pipe, a Vertex Detector capable of an impact parameter resolution of 3  $\mu\text{m}$  [26] is foreseen. Calorimetry at CLIC is based on fine-grained sandwich calorimeters optimized for particle-flow analysis (PFA). PFA is based on reconstruction of four-vectors of visible particles, combining the information from precise tracking with highly granular calorimetry. The detector comprises a central solenoid magnet, with a field of 4 T. High muon reconstruction efficiency of 99 %, for muons above 7.5 GeV, is achieved by combining information from the central tracker (TPC plus silicon tracker) with information provided by the iron yoke instrumented with the 9 layers of resistive plate chamber detectors.

In principle, hadrons produced in the interaction of the beam-induced photons affect the TPC occupancy and consequently the muon reconstruction efficiency. However, in the studied sample of muons from  $H \rightarrow \mu^+\mu^-$  decays, muon reconstruction efficiency is above 99 % in the barrel region, in the presence of  $\gamma\gamma \rightarrow$  hadrons.

The average muon transverse momentum resolution for the signal sample is  $\Delta(1/p_T) = 3.3 \times 10^{-5} \text{ GeV}^{-1}$  in the barrel region. The impact of transverse momentum resolution on the statistical uncertainty of  $\sigma(H\nu\bar{\nu}) \times \text{BR}(H \rightarrow \mu^+\mu^-)$  measurement is discussed in Sect. 9.

In the very forward region of the CLIC\_ILD detector, below  $\theta = 8^\circ$ , no tracking information is available. The region between  $0.6^\circ$  and  $6.3^\circ$  is instrumented with the two silicon-tungsten sampling calorimeters, LumiCal and BeamCal [27], for the luminosity measurement, beam-parameter control, as well as for the tagging of high-energy electrons escaping the main detector at low angles. Together with the very forward segments of the electromagnetic calorimeter covering the polar-angle region between  $6.3^\circ$  and  $8^\circ$ , it is possible to suppress the four-fermion SM background with the characteristic low-angle electron signature. The simulation of the very-forward electron tagging is described in Sect. 5.

## 4 Event samples

At  $\sqrt{s} = 1.4 \text{ TeV}$  the SM Higgs boson is predominantly produced via  $WW$ -fusion (Fig. 1). The effective cross-section for Higgs production in  $WW$ -fusion is 244 fb without beam

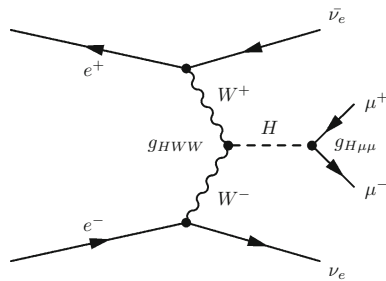


**Fig. 1** Feynman diagram of the Higgs production in  $WW$ -fusion and the subsequent Higgs boson decay to a pair of muons

polarization. The Higgs production cross-section above 1 TeV can be measured with a statistical precision better than 1 % as shown in [1]. The  $e^+e^- \rightarrow H\nu\bar{\nu}$ ,  $H \rightarrow \mu^+\mu^-$  signal statistics are expected to be small (of the order of a few tens of events) because of the small branching fraction for this particular decay.

We have simulated a sample of 24,000 signal events, roughly corresponding to 300 times the number of events expected in  $1.5 \text{ ab}^{-1}$  of data. This is needed in order to provide an adequate description of the signal probability density function (PDF) (Sect. 7.1). The signal and the dominant background processes are listed in Table 1. For each of the background processes, samples of  $2 \text{ ab}^{-1}$  are generated.

In addition to the processes listed in Table 1, we have considered s-channel  $e^+e^- \rightarrow \mu^+\mu^-$  production, as well as several processes with tau pair in the final state  $e^+e^- \rightarrow \tau^+\tau^-$ ,  $e^+e^- \rightarrow \nu_\tau\bar{\nu}_\tau\tau^+\tau^-$ ,  $e^+e^- \rightarrow e^-e^+\tau^+\tau^-$ . Tau decays become relevant if both taus decay into two muons which happens in  $\sim 3\%$  of cases [28]. However, the invariant mass of the di-muon system will not match the Higgs mass window considered in this analysis (see Sect. 6.1). The same

**Table 1** List of considered processes with corresponding cross-sections. Cross-section values marked by \* are generated with the additional kinematic requirements:  $100 \text{ GeV} < m_{\mu\mu} < 150 \text{ GeV}$ , and  $8^\circ < \theta_\mu < 172^\circ$ , where  $m_{\mu\mu}$  stands for di-muon invariant mass and  $\theta_\mu$  is the polar angle of the reconstructed muon. The cross-sections for all processes with photons in the initial state include interactions with Beamstrahlung photons ( $e\gamma_{\text{BS}}$  and  $\gamma_{\text{BS}}\gamma_{\text{BS}}$ ) as well as  $e^+e^-$  and  $e^\pm\gamma_{\text{BS}}$  processes modified with EPA when appropriate. Cross-sections for processes  $e^\pm\gamma \rightarrow e^\pm\mu^+\mu^-$  and  $e^\pm\gamma \rightarrow e^\pm\nu_\mu\bar{\nu}_\mu\mu^+\mu^-$  represent the sum of cross-sections for the processes with both initial states  $e^-\gamma$  and  $e^+\gamma$

Process	$\sigma(fb)$
$e^+e^- \rightarrow H\nu\bar{\nu}, H \rightarrow \mu^+\mu^-$	0.0522
$e^+e^- \rightarrow \nu\bar{\nu}\mu^+\mu^-$	129
$e^-e^+ \rightarrow e^-e^+\mu^+\mu^-$	24.5*
$e^\pm\gamma \rightarrow e^\pm\mu^+\mu^-$	1098*
$e^\pm\gamma \rightarrow e^\pm\nu_\mu\bar{\nu}_\mu\mu^+\mu^-$	30
$\gamma\gamma \rightarrow \nu_\mu\bar{\nu}_\mu\mu^+\mu^-$	162
$e^+e^- \rightarrow e^+e^-\nu_\mu\bar{\nu}_\mu\mu^+\mu^-$	1.6

holds for  $e^+e^- \rightarrow \mu^+\mu^-$  production. Misidentification of a pion as a muon is negligible, due to the fact that muon identification is performed not only by the muon detector but the central tracker, as well. In addition, hadronic events involving pions are further suppressed to a negligible level by kinematical selections.

$e^+e^-$  interactions as well as electron interactions with Beamstrahlung photon ( $e\gamma_{\text{BS}}$ ) are simulated using EPA, whenever the virtuality of the mediated photon is smaller than 4 GeV. In these cases  $e^+e^-$  interaction can be described as interaction of quasi-real photons  $\gamma_{\text{EPA}}$  ( $e^\pm\gamma_{\text{EPA}}, \gamma_{\text{EPA}}\gamma_{\text{EPA}}$ ). Similarly,  $e\gamma_{\text{BS}}$  can be described as  $\gamma_{\text{EPA}}\gamma_{\text{BS}}, \gamma_{\text{EPA}}\gamma_{\text{EPA}}$  when EPA is applicable. In this analysis, such events are grouped together with the processes involving Beamstrahlung photons. In this way, processes with roughly similar kinematic characteristics are grouped together, as shown in Table 1. The notation  $e^\pm\gamma$  represents the sum of cross-sections for the processes with either  $e^-\gamma$  or  $e^+\gamma$  in the initial state.

At  $\sqrt{s} = 1.4 \text{ TeV}$ , the Higgs boson is also produced via  $ZZ$ -fusion, with a cross-section of about 10 % of the Higgs production cross-section in  $WW$ -fusion. However, on a test sample of 300  $ZZ$ -fusion events followed by the Higgs decay to a pair of muons, not a single event passed the selection described in Sects. 6.1 and 6.2. This implies an efficiency smaller than 1.2 % (95 % CL) for this channel equivalent to less than 0.1 events passing the final selection. Therefore, the Higgs production through  $ZZ$ -fusion is not considered relevant for this analysis.

Photons, dominantly emitted by Beamstrahlung, produce incoherent pairs deposited mainly in the low-angle calorimeters. On average, 1.3 two-photon interactions producing hadronic final states occur per bunch crossing [29] which may affect the muon reconstruction in the tracking detectors. These hadrons are included in the analysis by overlaying 60 bunch crossings in the simulation, before the digitisation and event reconstruction phase. These events, as well as other physics events, are passed through the full detector simulation [30].

### 5 Tagging of EM showers in the very forward region

In the polar angle region below  $\theta = 8^\circ$ , tracking information and hadronic calorimetry are not available. The four-fermion background  $e^+e^- \rightarrow e^+e^-\mu^-\mu^+$  of multiperipheral type and similar processes like  $e^\pm\gamma \rightarrow e^\pm\mu^-\mu^+$  can fake the missing energy signature of the signal if the final state electrons (spectators), emitted at the polar angles smaller than  $\theta = 8^\circ$ , escape undetected.

Electron detection in the very forward region involves the reconstruction of electromagnetic showers in the presence of intense beam-induced background depositing in the very

**Table 2** Rejection rates for signal and background by the forward electron tagging

Process	Rejection rate (%)
$e^-e^+ \rightarrow e^-e^+\mu^+\mu^-$	48
$e^\pm\gamma \rightarrow e^\pm\mu^+\mu^-$	42
Signal	7

forward calorimeters a large number of low-energy particles, mostly incoherent pairs from Beamstrahlung [31]. This deposition amounts to several hundred thousand of  $e^+e^-$  pairs per bunch crossing [32].

Furthermore, Bhabha events where one or both electrons are detected in the very forward calorimeters may occur in coincidence with either signal or background, even within the 10 ns time stamp. Tagging of such Bhabha electrons will result in the rejection of signal (or background). In order to prevent significant loss of signal statistics, the electron tagging was optimized to identify showers with energy higher than 200 GeV and a polar angle above  $1.7^\circ$  only.<sup>1</sup> Under these requirements, the loss of the number of signal events due to tagging of Bhabha electrons amounts to 7%. Out of these 7%, in slightly more than a half of events one electron is added to the final state and, in the remainder two Bhabha electrons are added. Table 2 shows rejection rates for signal and background obtained by the forward electron tagging due to Bhabha pile-up.

In conclusion, very forward tagging of high-energy electrons serves to half the fraction of background with spectator electrons, with a moderate loss of signal of 7% in the presence of Bhabha coincidence.

## 6 Event selection

The event selection is done in two steps. First, a preselection is performed aiming to suppress background originating from beamstrahlung as well as the processes with spectator electrons described in Sect. 5. The final event selection uses a multivariate classifier based on boosted decision trees (BDT) to suppress remain background processes on the basis of their kinematic properties.

### 6.1 Preselection

In order to suppress the impact of the beam-induced background, only reconstructed particles with transverse momenta  $p_T > 5$  GeV are used in the analysis. Further-

<sup>1</sup> Simulation with the reconstruction algorithm from Ref. [33] shows that assuming these cuts, the reconstruction efficiency, in BeamCal and LumiCal is above 98%, with a negligible fake rate.

more, the preselection of events was made by requiring a reconstruction of exactly two muons in the event, with an invariant mass of the di-muon system in the window centered around the Higgs mass 105–145 GeV. In addition, the absence of tagged electrons with energy above 200 GeV and polar angle above  $1.7^\circ$  is required in order to suppress background with spectator electrons emitted in the very forward region of the detector.

### 6.2 MVA selection

As a second step in the event selection, MVA techniques are used based on the BDT classifier implemented in the TMVA package. From the signal sample, quarter of all events are reserved for TMVA training, as well as  $0.5 \text{ ab}^{-1}$  of each background. The following observables were used for the classification of events, similar to the CLIC study at  $\sqrt{s} = 3$  TeV [10]:

- visible energy of the event excluding the energy of the di-muon system,  $E_{\text{vis}}$ ,
- transverse momentum of the di-muon system,  $p_T(\mu\mu)$ ,
- scalar sum of the transverse momenta of the two selected muons,  $p_T(\mu_1) + p_T(\mu_2)$ ,
- boost of the di-muon system,  $\beta_{\mu\mu} = |p_{\mu\mu}|/E_{\mu\mu}$ ,
- polar angle of the di-muon system,  $\theta_{\mu\mu}$ ,
- cosine of the helicity angle,  $\cos\theta^*$ .

The process  $e^+e^- \rightarrow \nu\bar{\nu}\mu^+\mu^-$ , with the same final state as the signal, represents an irreducible background and can not be substantially suppressed before the invariant mass fit of the di-muon system. The process  $\gamma\gamma \rightarrow \nu_\mu\bar{\nu}_\mu\mu^+\mu^-$  has a similar final state, but a different CM energy distribution in the initial state, since it involves Beamstrahlung or EPA photons rather than initial electrons. This leads to a different distribution of the boost of the di-muon system, allowing separation from the signal to some extent. The processes  $e^+e^- \rightarrow \nu\bar{\nu}\mu^+\mu^-$  and  $\gamma\gamma \rightarrow \nu_\mu\bar{\nu}_\mu\mu^+\mu^-$ , have slightly different distributions of the helicity angle from the signal. All processes with one or two spectator electrons show significant differences from the signal, primarily in the distribution of the visible energy (Fig. 2). These processes are also effectively suppressed by the  $p_T(\mu_1) + p_T(\mu_2)$  observable. In addition, for the  $e^+e^- \rightarrow e^+e^-\mu^+\mu^-$  process, the distribution of  $p_T(\mu\mu)$  exhibits a peak at lower values than the signal (Fig. 3). This peak corresponds to events in which the di-muon system recoils against electron spectators or outgoing photons that are emitted below the angular cut of the very forward EM-shower tagging. The above is illustrated in Fig. 3 showing the  $p_T$  distributions for representative background processes.

The distribution of the BDT classifier variable for the signal and the main background processes is shown in Fig. 4a.

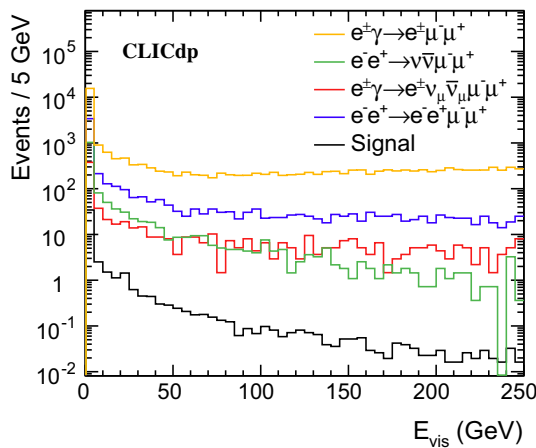


**Fig. 2** Distribution of the visible energy for the signal and  $e^\pm\gamma \rightarrow e^\pm\mu^+\mu^-$ ,  $e^+e^- \rightarrow \nu\bar{\nu}\mu^+\mu^-$ ,  $e^\pm\gamma \rightarrow e^\pm\nu_\mu\bar{\nu}_\mu\mu^+\mu^-$  and  $e^+e^- \rightarrow e^+e^-\mu^+\mu^-$  background

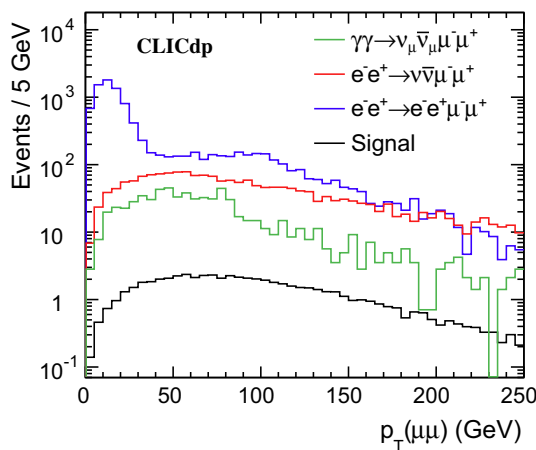


**Fig. 3** Distribution of the  $p_T(\mu\mu)$  for the signal and  $e^+e^- \rightarrow \nu\bar{\nu}\mu^+\mu^-$ ,  $\gamma\gamma \rightarrow \nu_\mu\bar{\nu}_\mu\mu^+\mu^-$ ,  $e^+e^+ \rightarrow e^+e^-\mu^+\mu^-$  background with spectator electrons

The classifier cut position was selected to maximise the significance, defined as  $N_s/\sqrt{N_s + N_b}$ , where  $N_s$  and  $N_b$  are the number of selected signal and background events, respectively. A plot of significance as a function of the position of the BDT cut is shown in Fig. 4b. The optimal cut position was found at BDT = 0.23. Distributions of the di-muon invariant mass before and after the MVA selection are shown in Fig. 5. Figure 5a includes all events that pass the preselection, while Fig. 5b shows all events passing the MVA selection. All samples are normalised to the integrated luminosity of  $1.5 \text{ ab}^{-1}$ . The signal preselection efficiency is 82 %. The MVA selection efficiency for the signal is 32 %, reflecting the fact that sensitive observables have limited power to discriminate between the signal and background. The overall signal efficiency including reconstruction, preselection, losses due to coincident tagging of Bhabha particles and the MVA is 24 %, resulting in an expected number of 19 signal events.

### 7 Di-muon invariant mass fit

The quantity  $\sigma(H\nu\bar{\nu}) \times BR(H \rightarrow \mu^+\mu^-)$  is determined from the equation:

$$\sigma(H\nu\bar{\nu}) \times BR(H \rightarrow \mu^+\mu^-) = \frac{N_s}{L \cdot \varepsilon_s} \tag{1}$$

where  $L$  stands for the integrated luminosity and  $\varepsilon_s$  is the total counting efficiency for the signal, including the reconstruction, preselection and MVA selection. In the experiment, the number of signal events  $N_s$  will be determined by fitting the di-muon invariant mass distribution with a function  $f(m_{\mu\mu})$ :

$$f(m_{\mu\mu}) = N_s f_s(m_{\mu\mu}) + N_b f_b(m_{\mu\mu}) \tag{2}$$

where  $f_{s,b}$  are probability density functions (PDF) used to describe the signal and the sum of all background processes, and  $N_s$  and  $N_b$  are the respective numbers of signal and background events in the fitting mass window. In this analysis, an unbinned likelihood fit, with all parameters of  $f_{s,b}(m_{\mu\mu})$  fixed, is performed on simulated signal and background samples.  $N_s$  and  $N_b$  are left as free parameters determined from the fit. The way the signal and background PDFs are obtained is discussed in Sect. 7.1.

In order to estimate the statistical uncertainty of the signal count, 5000 toy Monte Carlo (MC) experiments are performed, where pseudo-data are obtained by randomly picking the signal  $m_{\mu\mu}$  values from the fully simulated signal sample, while background  $m_{\mu\mu}$  values are randomly generated from the total background PDF  $f_b(m_{\mu\mu})$ . The size of the signal sample  $N'_s$  and sample sizes  $N'_{b,i}$  of individual backgrounds considered, are obtained from the Poisson distribution for the integrated luminosity of  $1.5 \text{ ab}^{-1}$ , taking into consideration corresponding cross-sections  $\sigma$  and the selection efficiencies  $\varepsilon$  ( $\langle N'_s \rangle = L \cdot \sigma_s \cdot \varepsilon_s$ ,  $\langle N'_{b,i} \rangle = L \cdot \sigma_i \cdot \varepsilon_i$ , where  $i$  is indexing the different background processes listed in Table 1).

For each toy MC experiment, the  $m_{\mu\mu}$  distribution is fitted by the function  $f(m_{\mu\mu})$  given in Eq. 2, and the standard deviation of the resulting distribution of  $N_s$  over all toy MC experiments is taken as the estimate of the statistical uncertainty of the  $\sigma(H\nu\bar{\nu}) \times BR(H \rightarrow \mu^+\mu^-)$  measurement.

As will be discussed in Sect. 9.1, the di-muon invariant mass distribution is sensitive to the detector  $p_T$  resolution, while the Higgs width  $\Gamma_H$  can be considered negligible in comparison to the detector energy resolution.

#### 7.1 Signal and background PDFs

Fully simulated samples of signal and background (Table 1) are fitted to extract the PDFs. The sizes of the samples vary from several tens of thousands of events for the signal, up to a few million of events for various background processes.

The signal PDF was defined as a linear combination of a Gaussian function with exponential tails,  $f_{exp}$  and a Gaus-

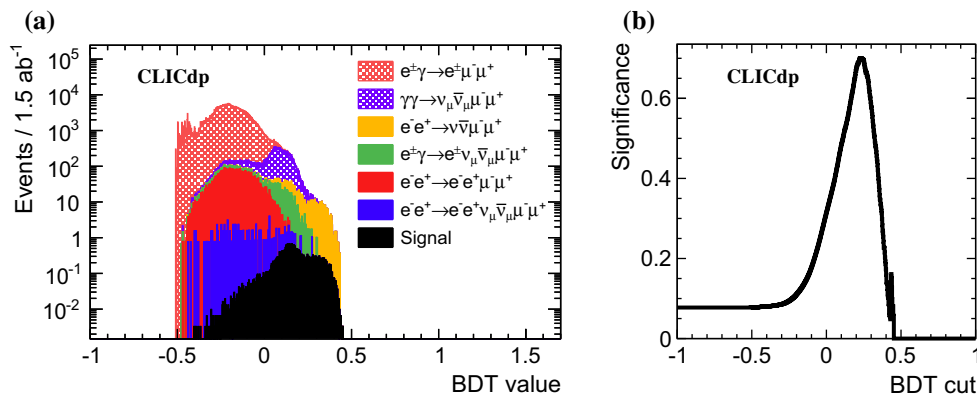


**Fig. 4** Stacked histograms of the BDT output variable for signal and background processes (a); Significance as a function of the BDT cut value (b)

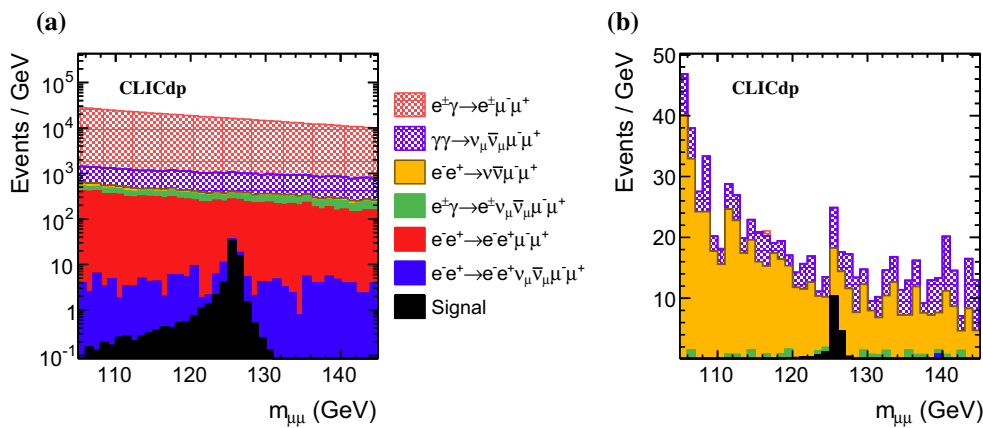


**Fig. 5** Stacked histograms of the di-muon invariant mass distributions with preselection only (a) and after MVA selection (b). The distributions are normalised to the same integrated luminosity of  $1.5 \text{ ab}^{-1}$ . The same legend applies to a, b

sian function with tails that asymptotically approach constant values in the high and low  $m_{\mu\mu}$ ,  $f_{flat}$ :

$$f_s = f_{flat} + C \cdot f_{exp} \quad \text{where}$$

$$f_{flat} = \begin{cases} e^{-\frac{(m_{\mu\mu}-m_H)^2}{2\sigma^2+\beta_L(m_{\mu\mu}-m_H)^2}} & m_{\mu\mu} < m_H \\ e^{-\frac{(m_{\mu\mu}-m_H)^2}{2\sigma^2+\beta_R(m_{\mu\mu}-m_H)^2}} & m_{\mu\mu} > m_H \end{cases} \quad \text{and}$$

$$f_{exp} = \begin{cases} e^{-\frac{(m_{\mu\mu}-m_H)^2}{2\sigma^2+\alpha_L|m_{\mu\mu}-m_H|}} & m_{\mu\mu} < m_H \\ e^{-\frac{(m_{\mu\mu}-m_H)^2}{2\sigma^2+\alpha_R|m_{\mu\mu}-m_H|}} & m_{\mu\mu} > m_H. \end{cases} \quad (3)$$

The parameters of Eq. 3 are determined by fitting the di-muon invariant mass distribution for the signal (Fig. 6).

The total background PDF is defined as a linear combination of a constant and exponential term:

$$f_b = p_0 \cdot (p_1 e^{p_2(m-m_H)} + (1 - p_1)) \quad (4)$$

The di-muon invariant mass fit of the total background is shown in Fig. 7, together with the fit results for the free

parameters in Eq. 4. As the normalisation to the common integrated luminosity requires different normalisation coefficients for different processes, binned data were used to combine the background processes in a straightforward manner and a binned  $\chi^2$  fit was performed. The  $\chi^2/N_{df}$  of the background fit was 62/61.

### 7.2 Distribution of the signal count

The overall function  $f(m_{\mu\mu})$  (Eq. 2) is fitted to the pseudo-data of each toy MC experiment using the unbinned likelihood fit. An example of a toy MC fit is given in Fig. 8.

The standard deviation of the resulting signal count distribution in 5000 repeated toy MC experiments corresponds to the statistical uncertainty of the measurement and is 38 %. (Fig. 9). According to Eq. 1 it translates into the statistical uncertainty of the  $\sigma(H\nu\bar{\nu}) \times BR(H \rightarrow \mu^+\mu^-)$  measurement, having in mind that the total uncertainty of the integrated luminosity can be determined at the permille level [34].

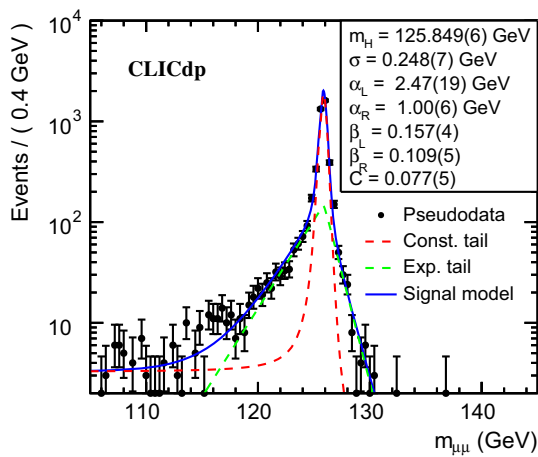


**Fig. 6** Distribution of the di-muon invariant mass  $m_{\mu\mu}$ , of the signal after MVA selection, used for the PDF determination. The distribution is fitted with the function  $f_s$  given in Eq. 3

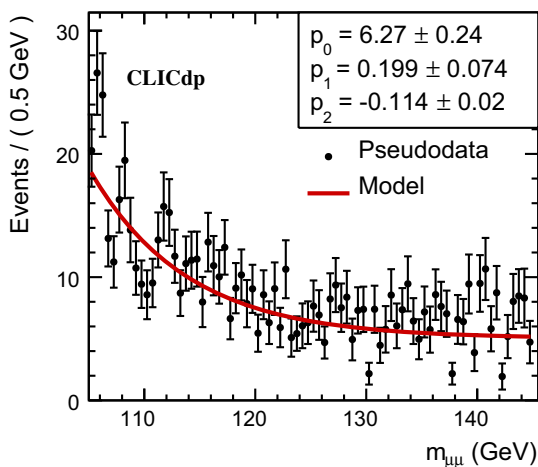


**Fig. 7** Distribution of the di-muon invariant mass  $m_{\mu\mu}$ , of the total background, after MVA selection. The distribution is fitted with the function  $f_b$  given in Eq. 4

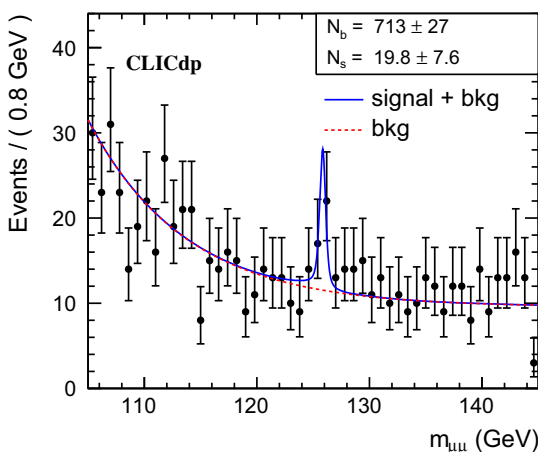


**Fig. 8** Fitted distribution of the di-muon invariant mass  $m_{\mu\mu}$ , for the sum of the signal and the total background in one toy MC experiment

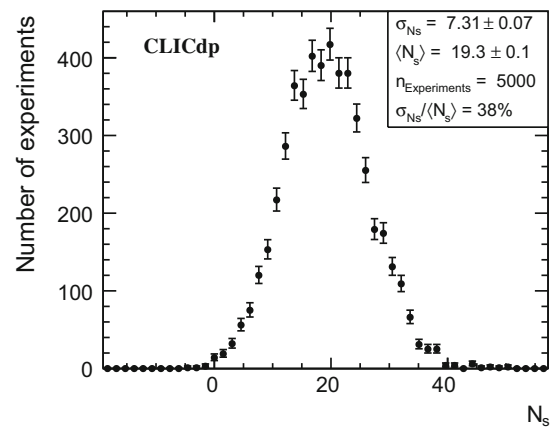


**Fig. 9** Distribution of the number of signal events in 5000 toy MC experiments

The statistical uncertainty of the signal counting is dominated by contributions from the limited signal statistics and from a presence of irreducible backgrounds. To estimate the significance of the signal against the null-hypothesis, another set of 5000 toy MC experiments was performed with zero signal count, and  $f(m_{\mu\mu})$  (Eq. 2) was fitted to the pseudo-data. The resulting  $N_s$  distribution was centered on zero with a standard deviation of 5.4. Thus, in the case where the SM expected number of 19 signal events are found in an experiment, the corresponding signal significance would be  $3.7\sigma$ .

The Higgs coupling to muons,  $g_{H\mu\mu}$ , is optimally extracted in a global fit procedure taking into account all Higgs measurements at the 350 GeV, 1.4 and 3 TeV stages. The global fit serves to extract Higgs couplings from all measurements, as well as the experimental Higgs width  $\Gamma_H$ . Because  $\sigma(H\nu\bar{\nu}) \times BR(H \rightarrow \mu^+\mu^-) \propto \frac{g_{HWW}^2 g_{H\mu\mu}^2}{\Gamma_H}$  and having access to  $\Gamma_H$  and  $g_{HWW}$  from other measurements, extraction of  $g_{H\mu\mu}$  is possible solely from the measurement presented here. An example of a minimal set of measurements giving a model-independent access to  $\Gamma_H$  and  $g_{HWW}$  is the following: the  $H \rightarrow b\bar{b}$  measurements at both 350 GeV and 1.4 TeV give access to the ratio  $\frac{g_{HWW}}{g_{HZZ}}$ , the recoil mass measurement at 350 GeV CM energy gives access to  $g_{HZZ}$ , and the  $H \rightarrow W^+W^-$  measurement at 1.4 TeV gives access to the ratio  $\frac{g_{HWW}^4}{\Gamma_H}$  [4]. The contributions of these measurements towards the final  $\Delta g_{H\mu\mu}$  is negligible at the second significant digit.

The dominant contribution to the  $g_{H\mu\mu}$  coupling uncertainty is the statistical uncertainty of the measurement presented here. Systematic uncertainties affect the total uncertainty of  $g_{H\mu\mu}$  determination only at the third significant digit, and thus can be neglected (Sect. 9). Under these assumptions, the relative uncertainty of  $g_{H\mu\mu}$  is approximated to be 19 %.

**Table 3** Summary of the  $\sigma(H\nu\bar{\nu}) \times BR(H \rightarrow \mu^+\mu^-)$  measurement at 1.4 TeV CLIC with unpolarised and 80 % polarized electron beams. All uncertainties are statistical

	Unpolarised	Polarised (80 %, 0 %)
$N_S$	$19.3 \pm 0.1$	$35 \pm 9$
$\varepsilon_S$	24 %	25 %
$\frac{\delta(\sigma(H\nu\bar{\nu}) \times BR(H \rightarrow \mu^+\mu^-))}{\sigma(H\nu\bar{\nu}) \times BR(H \rightarrow \mu^+\mu^-)}$	38 %	25 %
$\delta(g_{H\mu\mu})/g_{H\mu\mu}$	19 %	13 %

## 8 Impact of electron polarization

If 80 % left-handed polarisation of the electron beam is assumed during the entire operation time at 1.4 TeV, the Higgs production cross-section through  $WW$ -fusion would be enhanced by a factor 1.8 [4]. The most important background contribution after the MVA selection, the  $e^+e^- \rightarrow \nu_e\bar{\nu}_e\mu^+\mu^-$  process, is enhanced by the same factor because it is also mediated by  $W$  bosons which have only left-handed interactions. The process  $e^\pm\gamma \rightarrow e^\pm\mu^+\mu^-$  is enhanced by a factor 1.32, while cross-sections for other background processes are not significantly changed w.r.t. the unpolarised case. The overall selection efficiency of the signal is 25 %, because the classifier cut position is moved to a lower value which consequently leads to a higher signal efficiency. The final statistical uncertainty of the  $\sigma(H\nu\bar{\nu}) \times BR(H \rightarrow \mu^+\mu^-)$  measurement is 25 %. The corresponding uncertainty of  $g_{H\mu\mu}$  is 13 %. A summary of the results of the presented analysis is given in Table 3. It is important to note that all kinematic variables are unaffected by the beam polarization.

## 9 Systematic uncertainties

From Eq. 1 it is clear that uncertainties of the integrated luminosity and muon identification efficiency influence the uncertainty of the  $H \rightarrow \mu^+\mu^-$  branching ratio measurement at the systematic level. It has been shown that at 3 TeV CLIC [35], where the impact of the beam-induced processes is the most severe, the luminosity above 75 % of the nominal CM energy can be determined at the permille level, using low-angle Bhabha scattering. Below 75 % of the nominal CM energy, the luminosity spectrum can be measured with a precision of a few percent using wide-angle Bhabha scattering [36]. About 17 % of all Higgs production events occur at a CM energy below 75 % of the nominal CM energy. Having in mind the intrinsic statistical limitations of the signal sample, this source of systematic uncertainty can be considered negligible.

On the detector side, an important systematic effect is the uncertainty on the transverse momentum resolution, because

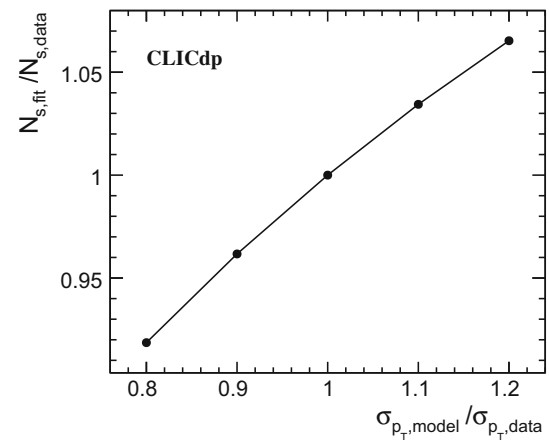


**Fig. 10** Impact of the uncertainty of the muon  $p_T$  resolution on the signal counting. The relative shift of the signal count is given as a function of the relative shift of the  $p_T$  resolution

it directly influences the expected shape of the signal  $m_{\mu\mu}$  distribution. The sensitivity of the signal count to the accuracy of the knowledge of the  $p_T$  resolution  $\sigma_{p_T}$  has been studied by performing the analysis with an artificially introduced uncertainty of an exaggerated magnitude on the assumed  $p_T$  resolution used to extract the signal PDF. Results of the relative shift in signal counts w.r.t. the relative shift of  $\sigma_{p_T}$  are shown in Fig. 10. The relative bias in signal counting per one percent change of  $\sigma_{p_T}$  is 0.35 %.

The uncertainty of the muon identification efficiency will directly influence the signal selection efficiency. In addition, the uncertainty of the muon polar angle resolution impacts the  $m_{\mu\mu}$  reconstruction. Based on the results of the LEP experiments [37], it can be assumed that these detector related uncertainties are below a percent.

The systematic uncertainty of the signal count caused by the fit with  $f_{m_{\mu\mu}}$  defined in Eq. 2, was found to be about 1 % which is small compared to the statistical error.

Because of the forward EM shower tagging, about 7 % of all events are rejected by coincident detection of Bhabha events. This fraction must be precisely calculated taking into account Bhabha event distributions, beam-beam effects, as well as the dependence of the tagging efficiency on energy and angle of the incident electrons and photons. This is work in progress [38–40], but the uncertainty of this effect is also expected to be negligible compared to the statistical uncertainty of the measurement.

### 9.1 Benefit of a improved $p_T$ resolution

To estimate the benefit of a better  $p_T$  resolution, the analysis was repeated by substituting the muon four-momenta reconstructed in the full simulation of the signal by the four-momenta obtained by a parametrisation of the momentum resolution for several different values of the detector



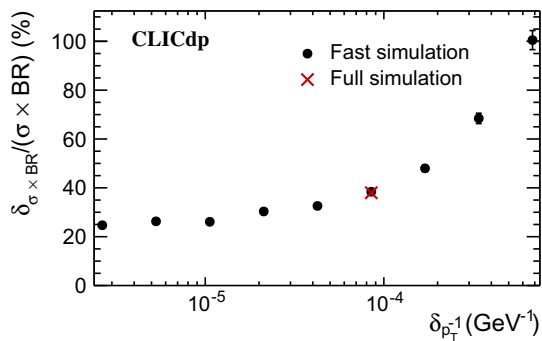


**Fig. 11** Dependence of the relative statistical uncertainty of the  $\sigma(H\nu\bar{\nu}) \times BR(H \rightarrow \mu^+\mu^-)$  on the transverse momentum resolution,  $\delta_{1/p_T}$ , averaged over the signal sample in the whole detector

resolution. Figure 11 displays the approximate dependence of the statistical uncertainty of the measurement on the average transverse momentum resolution in the whole detector. For this particular measurement, due to the limited statistics of signal, even a large improvement of the muon momentum resolution would result in only a moderate improvement of the statistical uncertainty of the measured product of the Higgs production cross-section and the branching ratio for the  $H \rightarrow \mu^+\mu^-$  decay.

## 10 Conclusions

It has been shown that the measurement of the cross-section times the branching ratio for the SM Higgs decay into two muons can be performed with a relative statistical uncertainty of 38 % at 1.4 TeV CLIC, assuming  $1.5 \text{ ab}^{-1}$  integrated luminosity with unpolarised beams. The result is dominated by the limited signal statistics and the irreducible background. The systematic uncertainties are negligible in comparison to the statistical one. This translates into a relative uncertainty of the coupling of Higgs to muons  $g_{H\mu\mu}$  of approximately 19 %. If the same integrated luminosity is collected with 80 % left-handed polarisation for the electrons, the relative statistical uncertainty improves to 25 and 13 % for  $\sigma(H\nu\bar{\nu}) \times BR(H \rightarrow \mu^+\mu^-)$  and  $g_{H\mu\mu}$ , respectively.

**Acknowledgments** The authors would like to thank the members of the analysis working group in the CLICdp collaboration for useful discussions. Konrad Elsener, Aharon Levy, Sophie Redford and Eva Sickling are especially acknowledged for carefully reading the manuscript. The production of the investigated event samples would not have been possible without the support from Stephane Poss and Andre Sailer. We acknowledge the support received from the Ministry of Education, Science and Technological Development of the Republic of Serbia within the project OI171012.

**Open Access** This article is distributed under the terms of the Creative Commons Attribution 4.0 International License (<http://creativecommons.org/licenses/by/4.0/>), which permits unrestricted use, distribution,

and reproduction in any medium, provided you give appropriate credit to the original author(s) and the source, provide a link to the Creative Commons license, and indicate if changes were made. Funded by SCOAP<sup>3</sup>.

## References

1. R.S. Gupta, H. Rzehak, J.D. Wells, How well do we need to measure Higgs boson couplings? *Phys. Rev. D* **86**, 095001 (2012). [arXiv:1206.3560](https://arxiv.org/abs/1206.3560)
2. C. Englert, et al., Precision measurements of higgs couplings: implications for new physics scales, *J. Phys. G* **41**, 113001 (2014). [arXiv:1403.7191](https://arxiv.org/abs/1403.7191)
3. L. Linssen, et al., ed., Physics and detectors at CLIC: CLIC Conceptual Design Report, ANL-HEP-TR-12-01, CERN-2012-003, DESY 12-008, KEK Report 2011-7, CERN, 2012. [arXiv:1202.5940](https://arxiv.org/abs/1202.5940)
4. H. Abramowicz, et al., Physics at the CLIC e+e- linear collider-input to the snowmass process. (2013). [arXiv:1307.5288](https://arxiv.org/abs/1307.5288)
5. S. Dittmaier, et al., Handbook of LHC higgs cross sections: 2. differential distributions. (2012). [arXiv:1201.3084](https://arxiv.org/abs/1201.3084)
6. Search for the standard model Higgs boson decay to  $\mu^+\mu^-$  with the ATLAS detector. (2014). [arXiv:1406.7663](https://arxiv.org/abs/1406.7663)
7. J. Hugon for the CMS Collaboration, Search for the standard model Higgs boson decaying to  $\mu^+\mu^- = 7$  and 8 TeV. CMS-CR-2014-189. (2014). [arXiv:1409.0839](https://arxiv.org/abs/1409.0839)
8. P. Lebrun, et al., ed., The CLIC Programme: towards a staged e+e- linear collider exploring the Terascale, ANL-HEP-TR-12-51, CERN-2012-005, KEK Report 2012-2, MPP-2012-115, CERN (2012)
9. D. Dannheim, P. Lebrun, L. Linssen, D. Schulte, F. Simon, S. Stapnes, N. Toge, H. Weerts, J. Wells, CLIC  $e^+e^-$  linear collider studies. (2012). [arXiv:1208.1402](https://arxiv.org/abs/1208.1402)
10. C. Grefe, T. Laštovička, J. Strube, Prospects for the measurement of the Higgs Yukawa couplings to b and c quarks, and muons at CLIC. *Eur. Phys. J. C* **73**, 2290 (2013)
11. C.F. von Weizsäcker, Radiation emitted in collisions of very fast electrons. *Z. Phys.* **88**, 612 (1934)
12. E.J. Williams, Nature of the high-energy particles of penetrating radiation and status of ionization and radiation formulae. *Phys. Rev.* **45**, 729 (1934)
13. W. Kilian, T. Ohl, J. Reuter, WHIZARD: simulating multi-particle processes at LHC and ILC. *Eur. Phys. J. C* **71** (2011)
14. M. Moretti, T. Ohl, J. Reuter, O'Mega, An optimizing matrix element generator. LC- TOOL 2001-040 (2001)
15. T. Sjostrand, S. Mrenna, P. Z. Skands, PYTHIA 6.4 Physics and Manual, *JHEP* **05**, 026 (2006). [arXiv:hep-ph/0603175](https://arxiv.org/abs/hep-ph/0603175)
16. D. Schulte, Beam-beam simulations with GUINEA-PIG, CERN-PS-99-014-LP (1999)
17. Z. Was, TAUOLA the library for tau lepton decay, and KKMC/KORALB/KORALZ/... status report, *Nucl. Phys. Proc. Suppl.* **98**, 96 (2001). [arXiv:hep-ph/0011305](https://arxiv.org/abs/hep-ph/0011305)
18. P. Mora de Freitas, H. Videau, Detector simulation with Mokka/Geant4: present and future, international workshop on linear colliders (LCWS 2002), LC-TOOL-2003-010, JeJu Island, Korea (2002)
19. S. Agostinelli et al., Geant4—a simulation toolkit. *Nucl. Instrum. Methods Phys. Res. Sect. A* **506**, 250 (2003)
20. M.A. Thomson, Particle flow calorimetry and the PandoraPFA algorithm. *Nucl. Instrum. Methods A* **611**, 25 (2009). [arXiv:0907.3577](https://arxiv.org/abs/0907.3577)
21. J. Marshall, A. Münnich, M. Thomson, Performance of particle flow calorimetry at CLIC. *Nucl. Instrum. Methods A* **700**, 153 (2013). [arXiv:1209.4039](https://arxiv.org/abs/1209.4039)

22. O. Wendt, F. Gaede, T. Kramer, Event reconstruction with Marlin-Reco at the ILC. *Pramana* **69**, 1109 (2009). [arXiv:physics/0702171](https://arxiv.org/abs/physics/0702171)
23. A. Höcker, et al., TMVA—toolkit for multivariate data analysis. (2009). [arXiv:physics/0703039](https://arxiv.org/abs/physics/0703039)
24. T. Abe, et al., The international large detector: letter of intent. (2010). [arXiv:1006.3396](https://arxiv.org/abs/1006.3396)
25. A. Münnich, A. Sailer, The CLIC\_ILD\_CDR geometry for for the CDR Monte Carlo mass production. CERN LCD-Note-2011-002 (2011)
26. D. Dannheim, Vertex-detector R&D for CLIC, CLICdp-Conf-2014-004 (2014)
27. H. Abramowicz, et al., Forward instrumentation for ILC detectors. *JINST* **5**, P12002 (2010). [arXiv:1009.2433](https://arxiv.org/abs/1009.2433)
28. K.A. Olive, et al., Review of particle physics. *Chin. Phys. C* **38**, 090001 (2014)
29. T. Barklow, D. Dannheim, O. Sahin, D. Schulte. Simulation of  $\gamma\gamma$  to hadrons background at CLIC. CERN LCD-Note-2011-020 (2011)
30. P. Schade, A. Lucaci-Timoce, Description of the signal and background event mixing as implemented in the Marlin processor OverlayTiming. CERN LCD-Note-2011-006 (2011)
31. D. Dannheim, A. Sailer, Beam-induced backgrounds in the CLIC detectors. LCD-Note-2011-021 (2011)
32. P. Chen, Beamstrahlung and the QED, QCD backgrounds in linear colliders. SLAC-PUB-5914 (1992)
33. A. Sailer, Electron Tagging with the BeamCal at 3 TeV CLIC, Linear Collider Workshop, Arlington, Texas. (2012). <https://agenda.linearcollider.org/event/5468/session/12/contribution/176/material/slides>
34. R. Schwartz, Luminosity measurement at the compact linear collider. CERN-THESIS-2012-345 (2012)
35. S. Lukić, et al., Correction of beam-beam effects in luminosity measurement in the forward region at CLIC. *JINST* **8**, P05008 (2013). [arXiv:1301.1449](https://arxiv.org/abs/1301.1449)
36. S. Poss, A. Sailer, Luminosity spectrum reconstruction at linear colliders. *Eur. Phys. J. C* **74**, 2833 (2014)
37. S. Schael, et al., Precision electroweak measurements on the Z resonance, *Phys. Rep.* **427**, 257 (2006), [arXiv:hep-ex/0509008](https://arxiv.org/abs/hep-ex/0509008)
38. V. Makarenko, Status of new generator for Bhabha scattering, in *Presented at the CLIC workshop, CERN* (2014). <https://indico.cern.ch/event/275412/session/5/contribution/183/material/slides>
39. A. Sailer, Status Report on forward region studies at CLIC, in *Presented at the CLIC workshop, CERN* (2014). <https://indico.cern.ch/event/275412/session/5/contribution/171/material/slides>
40. S. Lukić, Forward electron tagging at ILC/CLIC, in *Presented at the CLIC workshop, CERN* (2014). <https://indico.cern.ch/event/275412/session/5/contribution/172/material/slides>